JOURNAL OF CATALYSIS 147, 429–440 (1994)

# Interaction of Nickel Deposits with Catalytic Metals on $CoMo/Al_2O_3$ Hydrodemetallation Catalysts

Xinjin Zhao[1] and James Wei[2]

*Department of Chemical Engineering, Massachusetts Institute of Technology, Cambridge, Massachusetts, 02139*

Received January 28, 1993; revised December 13, 1993

**The structures of nickel deposits on sulfided $CoMo/Al_2O_3$ hydrodemetallation catalyst surface were characterized by using scanning transmission electron microscopy and high-resolution transmission electron microscopy techniques to study the interaction between the deposits and catalytic components. The deposits were found in crystallite form of nickel sulfide ($Ni_7S_6$) on the catalyst surface. Within the crystallites cobalt is uniformly distributed. Molybdenum is only partially associated with the nickel deposits as a segregated surface layer of molybdenum sulfide ($MoS_2$). For crystallites smaller than about 15 nm, the extent of segregation decreases. About 75% of the molybdenum is not directly associated with nickel deposits. Extensive cover-up of molybdenum by nickel deposits was not observed, and is not the main reason of catalyst deactivation. It was found that nickel deposits migrated towards cobalt sites even though molybdenum sites were the active sites for the hydrodemetallation reaction. Structure affinity favored the formation of solid solution between cobalt and nickel sulfides, which was the driving force for the association between nickel and cobalt on the catalyst surface. Microscopic characterization showed that deposition of nickel sulfide on the catalyst surface enhanced the mobility of the catalytic components $MoS_2$. Coalescence of $MoS_2$ leads to significant reduction of accessible molybdenum sulfide sites, and is the main reason for the deactivation of hydrodemetallation catalyst.** © 1994 Academic Press, Inc.

## INTRODUCTION

Deactivation of hydrodemetallation catalyst has been studied extensively due to the demand for the processing of increasing amounts of resid and low quality crude oils. However, the interaction between metal deposits and the catalyst, and its implications on catalyst deactivation, are still not well understood. The metal deposits on catalyst surface are increasingly found to take place as crystallites (1–3) over discrete sites rather than as uniform layers.

Toulhoat *et al.* (3) used scanning transmission electron microscopy (STEM) fitted with an X-ray analyzer, transmission electron microscopy (TEM), electron microprobe (EMPA), and X-ray diffraction analyzer (XRD) to analyze catalyst aged with a heavy industrial feed stock, pentane deasphalted Boscan crude. The deposits were identified to be $V_3S_4$ with the presence of nickel. Deoposited crystallite diameters observed were 20 to 40 nm near the edge of the catalyst and 5 to 10 nm near the center. However, it was found that the number of crystallites did not change significantly from the edge to the center of the catalyst.

Smith and Wei (2, 4, 5) studied hydrodemetallation with model compounds of nickel and vanadyl porphyrins with clean oil at 553–623 K. The study was conducted with a commercial $CoMo/Al_2O_3$ catalyst, HDS16A. The aged catalysts were studied extensively with transmission electron microscopy. Other techniques, including scanning electron microscopy, X-ray diffraction analyzer, X-ray photoelectron spectroscopy (XPS), were also used in the study. Smith and Wei found that, for a given hydrotreating catalyst aged at a given set of operating conditions, the number of nickel sulfide crystallites remained relatively constant, while the size of these crystallites grew with nickel sulfide loading. The sizes of these crystallites grew from 10 to 15 nm, while the metal loading was increased from 3 wt.% to about 100 wt%.

Resorting to X-ray elemental mapping, we showed that nickel deposits are strongly associated with cobalt on the catalyst surface, but not with molybdenum (6). Since molybdenum sulfide on sulfided $CoMo/-Al_2O_3$ is generally considered to be the active component for hydrotreating reactions, it is important to know how the nickel deposits interact with molybdenum on the surface. The objectives of this work are to characterize the structure of the deposits and the interaction between the deposits and the catalytic metals, especially the distribution of molybdenum on the aged catalyst surface, and to attempt to understand the mechanism for the formation and development of the structure of the nickel deposits on aged hydrodemetallation catalyst surfaces, and the implications to catalyst deactivation.

[1] Present address: W. R. Grace & Co.-Conn., Washington Research Center, 7379 Route 32, Columbia, MD 21044.

[2] To whom correspondence should be addressed. Present address: School of Engineering and Applied Sciences, Princeton University, Princeton, NJ 08544-5263.



0021-9517/94 $6.00

TABLE 1

Catalyst Properties

| | Mo (wt.%) | Co (wt.%) | P (wt.%) | Surface area ($m^2/g$) |
|---|---|---|---|---|
| HDS16A | 8.13 | 4.48 | 3.0 | 176 |
| SN6931 | 5.09 | 2.87 | 2.21 | 171 |

## EXPERIMENTAL AND CHARACTERIZATION

Two presulfided $CoMo/\gamma Al_2O_3$ catalysts were used for the hydrodemetallation experiments. The principal catalyst was a commercial $CoMo/Al_2O_3$ catalyst American Cyanamid Aero HDS16A, which contains 12.2 wt.% of $MoO_3$ and 5.7 wt.% of CoO. The other catalyst SN6931 was provided by American Cyanamid specifically for this work. It contains about 7.64 wt.% of $MoO_3$ and 3.65 wt.% of CoO. Both of the catalysts were prepared by impregnating metals from aqueous solutions. Properties of the catalysts are listed in Table 1. The catalysts were supplied in oxide form as extrudates and were crushed to about 78–80 $\mu$m for the hydrodemetallation to ensure the absence of intraparticle diffusion limitation. HDS16A has a surface area of 176 $m^2/g$ and a unimodal pore size distribution with a median pore diameter of 8.04 nm.

The catalyst sulfiding was carried out *in situ* by a 10 mol% hydrogen sulfide/hydrogen gas mixture (Matheson Gas Products) at a flow rate of about 150 ml/min, according to a standard temperature program recommended by American Cyanamid. The temperature was held at 448 K for 6 h, then raised to the desired reaction temperature at a rate of 60 K/min, then maintained at that temperature for 1 h.

The hydrodemetallation experiment was conducted in a 1-liter batch reactor (Autoclave Engineers, Model AFP 1005). The reactor system has been described previously by Smith and Wei (4). Modification to the reactor includes a sintered stainless steel basket to hold the catalysts inside the reactor. The nominal pore size of the basket was about 7 $\mu$m. The basket was attached to the end of the stirrer by a specially designed holder. Since the sizes of the porphyrin molecules are only about 1–1.2 nm, the basket does not block the free access of the porphyrin molecules to the catalysts. Nickel etio-porphyrin was used as the model compound, which is present in resid oil and typically comprises 10–50% of the metals found in crude oils (7). Squalane (supplied by Sigma Chemical Co.) was used as the liquid carrier for metal porphyrins in the hydrodemetallation experiments. It consists of 97.4% *iso*-paraffins, and a small amount of naphthenes and aromatics.

Operating conditions for the hydrodemetallation experiments range from 588 to 623 K at hydrogen pressure of 4.8 MPa and hydrogen sulfide partial pressure at about 14 kPa (0.3 vol.%). It should be noted that the hydrogen sulfide concentration was not very precisely controlled. It could range from about 0.2 to 0.5%.

After each hydrodemetallation experiment, aged catalysts with the stainless steel basket were taken out of the reactor and transferred to a glove box filled with argon. During the transfer process, the sample was kept under the cover of solvent. The samples were then washed repeatedly with xylene and acetone, and dried in a self-sealing crucible before any samples for characterization were prepared. The specimens for electron microscopy study were prepared by ultramicrotomy. The aged catalyst sample was embedded in an ultra-low viscosity resin provided by Ladd Research Industries, Inc. The resin block with catalyst samples was then cut with a glass knife and a diamond knife to get specimens with a thickness of about 60 to 80 nm. After the thin slices of specimens were loaded in copper grid, they were carbon coated for increasing conductivity before microscopic studies were conducted. The samples for TEM and STEM were virtually the same, though a thicker carbon coating was needed for STEM to facilitate the X-ray analysis.

The major characterization tool was a dedicated scanning transmission electron microscopy (Vacuum Generator HBO) equipped with Link energy dispersive X-ray analyzer. It offers a unique approach for measuring individual small crystallites which may be catalytically active as opposed to the averaging method employed in spectroscopic techniques. The X-ray mapping and EDS spectra were obtained at 100 kV, with a nominal probe size of about 2 nm.

High-resolution transmission electron microscopy (HRTEM) was used in the present work for studying the interaction of the nickel deposits with catalytic metal on the atomic level. It is the only technique that can make possible the direction description of the microstructure of solids in real space. The study was carried out on an Akashi Topcon EM002B (Akashi Beam Technology Corporation) with a point to point resolution of 0.18 nm (200 keV).

During the TEM and STEM analyses, care was taken to ensure that characterized areas and particles were representative of the catalyst samples. Typically, specimens were thoroughly examined at low magnification for any inhomogeneity.

## STRUCTURE OF DEPOSITS

### *Characterization by STEM*

Element distributions within the crystallites were studied by using scanning transmission electron microscopic technique. The aim is to detect element distributions

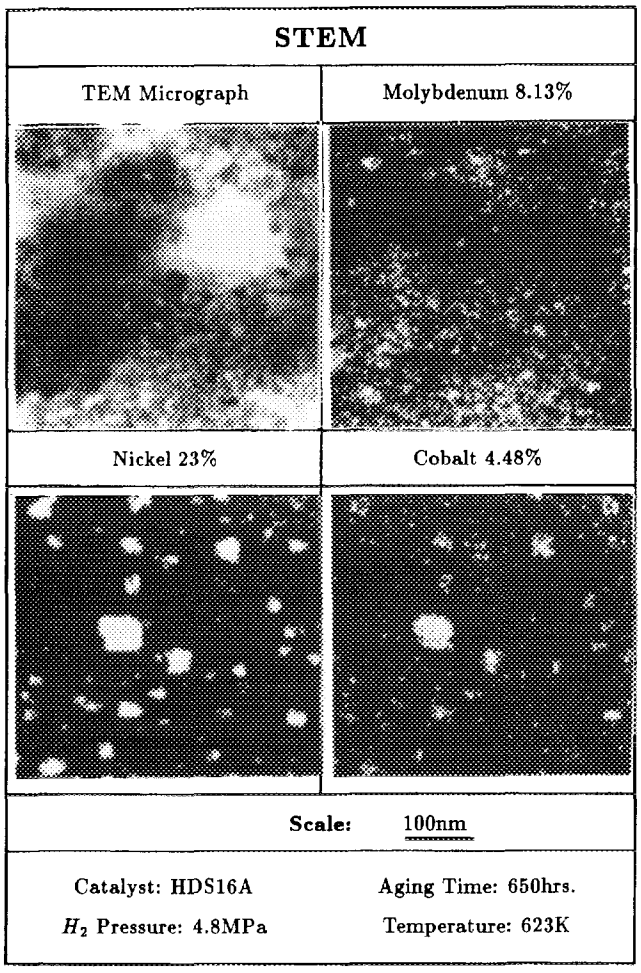


FIG. 1. Elemental mapping of aged HDS16A catalyst.

within the crystallite, or surface enrichment of one component. If the elements are uniformly distributed within the crystallites, we should get the same element ratios when we analyze the center or the edge of the crystallites. On the other hand, if there is an element enriched on the surface of the crystallites, we will get different element ratios at different analyzing positions.

The first sample we analyzed was an aged catalyst HDS16A sample, which is loaded with 23 wt.% nickel. To facilitate the analysis, we magnified the sample $\times 1{,}000{,}000$, and obtained the best resolution we could, and then scanned the specimen to locate some large crystallites.

Figure 1 shows a micrograph and elemental mapping of one area we examined. Crystallite A is located left of the center, and measures about 50 nm. We can clearly see the association between nickel and cobalt. To analyze the elemental distribution within the crystallite, we first focused the electron probe on the very edge of crystallite and conducted XEDS analysis, which continued for 100 s. During the analysis, we would check sample drifting every 20 s to make sure the probe was still on the original position. After the analysis was complete, we moved onto another position.

The analysis results are plotted in Fig. 2 for the 15 positions analyzed on crystallite A. The circles indicate the positions analyzed, and the numbers are the ratios of cobalt or molybdenum to nickel content at that position. Clearly, there is a significant difference between the distributions of cobalt and molybdenum. Although cobalt is virtually uniform throughout the whole crystallite, molybdenum is strongly enriched on certain surfaces of the crystallites. The results are also plotted in Fig. 3 as element ratios vs relative distances from the center of the crystallite. The overall molar ratio of cobalt to nickel within the crystallite is about 0.18. Considering the small area analyzed, it is very close to the bulk molar ratio of 0.2. On the other hand, the molybdenum to nickel ratio is much lower than the bulk molar ratio of about 0.22. These results indicate that much of the cobalt on the catalyst is associated with nickel, while only part of the molybdenum is associated with the nickel deposits at the surface of the deposits. The rest of the molybdenum is not associated with nickel at all. We also noted that the molybdenum enrichment only occurred at certain particular surfaces, rather than every surface of the nickel deposits.

Figure 2 also includes the analysis results for crystallite B from aged catalyst SN6931. Cobalt is again distributed throughout the crystallite, while molybdenum has a much higher concentration on some surfaces. The results are plotted in Fig. 4. Again, the molar ratio of cobalt to nickel is close to the bulk ratio of 0.13, while the molybdenum-to-nickel molar ratio is much lower than the bulk ratio of 0.14.

To make sure the analyzed crystallites are representative of the nickel deposits, and the results represent at least a qualitative trend, we analyzed more crystallites in catalyst HDS16A with different sizes ranging from about 6 to 60 nm. The results are plotted in Figs. 5 and 6. Once again, the ratio of cobalt to nickel is close to the bulk ratio of 0.2, while the molybdenum-to-nickel ratio only accounts for about 25% of the bulk molybdenum to nickel ratio.

Another interesting observation was made for the crystallites with different sizes. Similar to a two-component system, we define the ratio

$$\chi = (X^{\text{surface}}/X^{\text{center}})_A/(X^{\text{center}}/X^{\text{surface}})_B$$

as the surface enrichment factor as in a binary system, where A represents the catalytic metals cobalt or molybdenum, and B represents the nickel deposits.

When we plot the surface enrichment factor against the

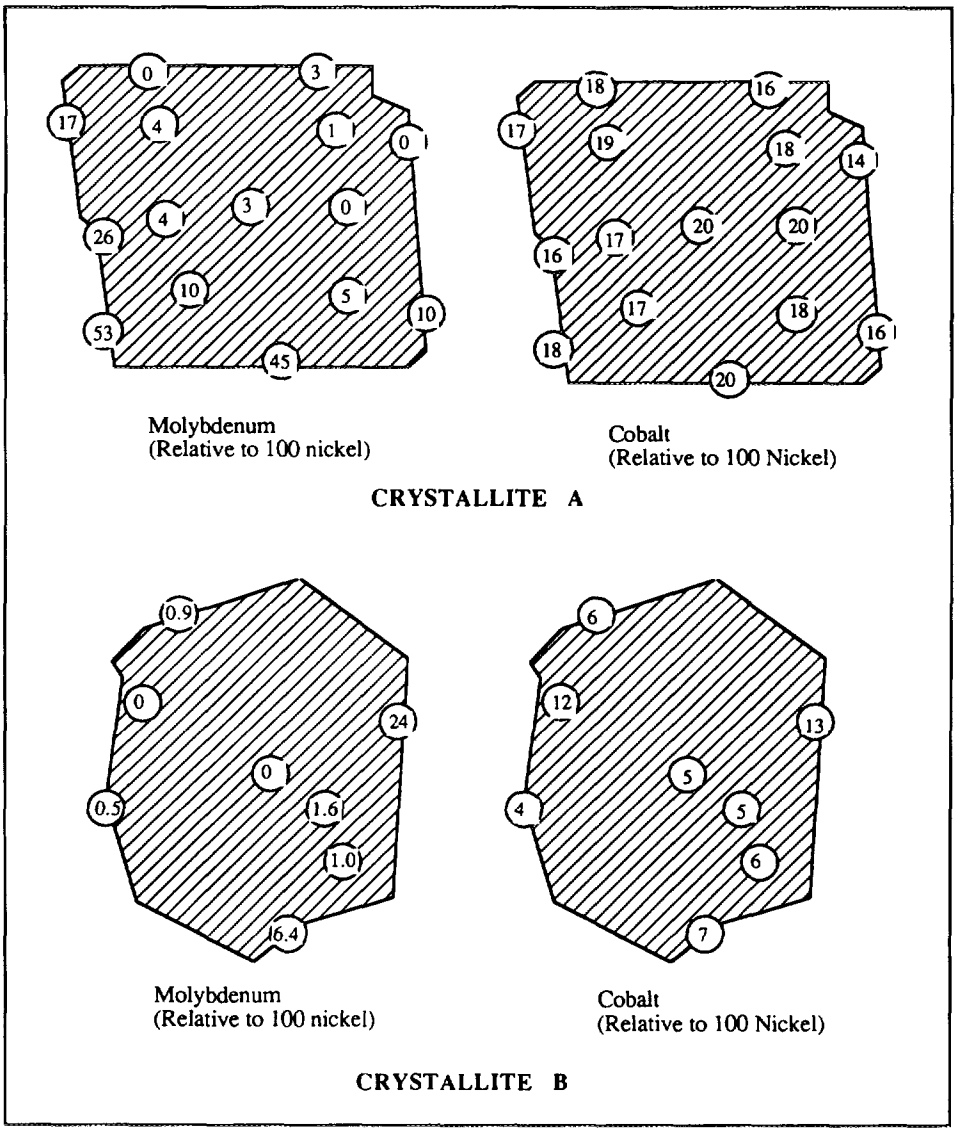


FIG. 2. Element molar ratios within crystallites.

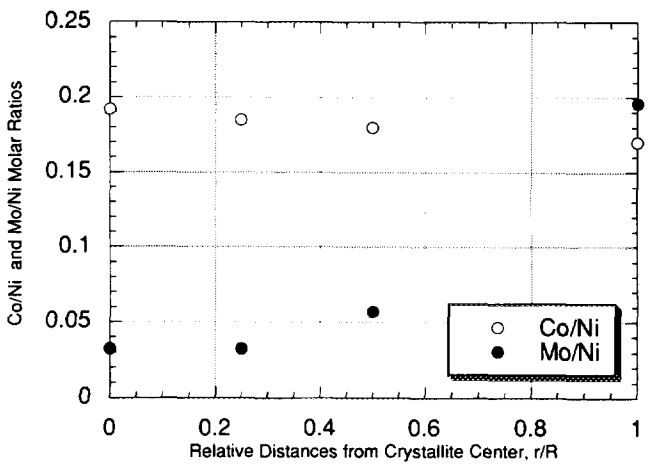


FIG. 3. Element distribution within crystallite A.

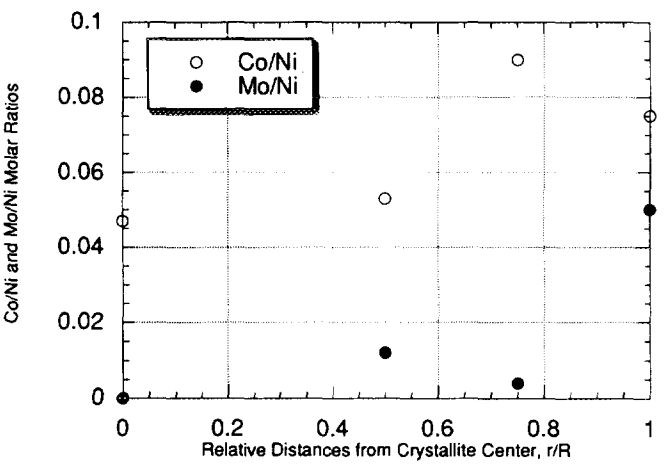


FIG. 4. Element distribution within crystallite B.

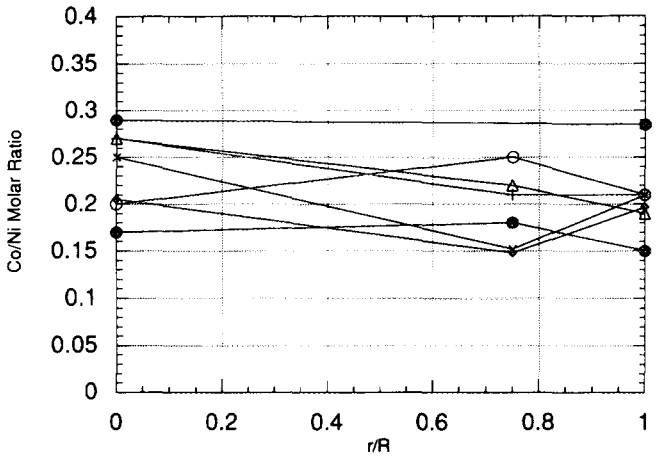


FIG. 5. Cobalt/nickel radial distribution within crystallites.

sizes of the crystallites in Fig. 7, it is clear that cobalt is uniformly distributed with the crystallites regardless of the sizes of the crystallites, indicated by the fact that the enrichment factor is distributed evenly around 1. Molybdenum, however, has a much higher concentration on the surface, though the enrichment factor decreases for crystallites smaller than about 15 nm. This is consistent with the theoretical calculations by Helms (8), which showed that the effect of particle size on segregation could be very significant, depending on the magnitude of the heat of segregation. Intuitively, as the particle size approaches zero, the surface composition must approach the bulk value. For crystallites smaller than about 5 nm, we were limited by the resolution of the scanning transmission electron microscope. In addition, the drifting of the samples also causes difficulties for the analysis of even smaller particles.

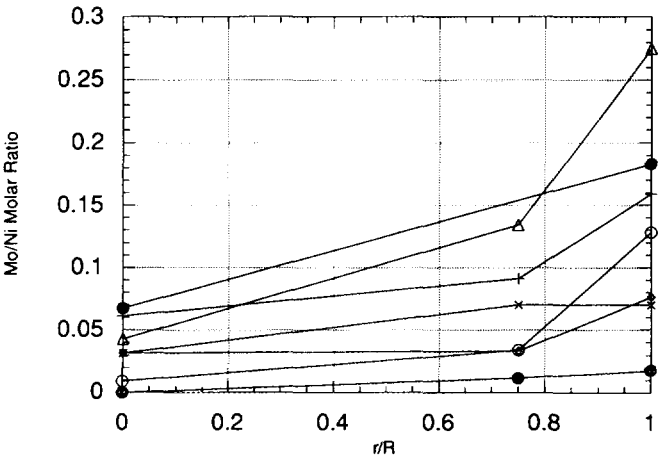


FIG. 6. Molybdenum/nickel radial distribution within crystallites.

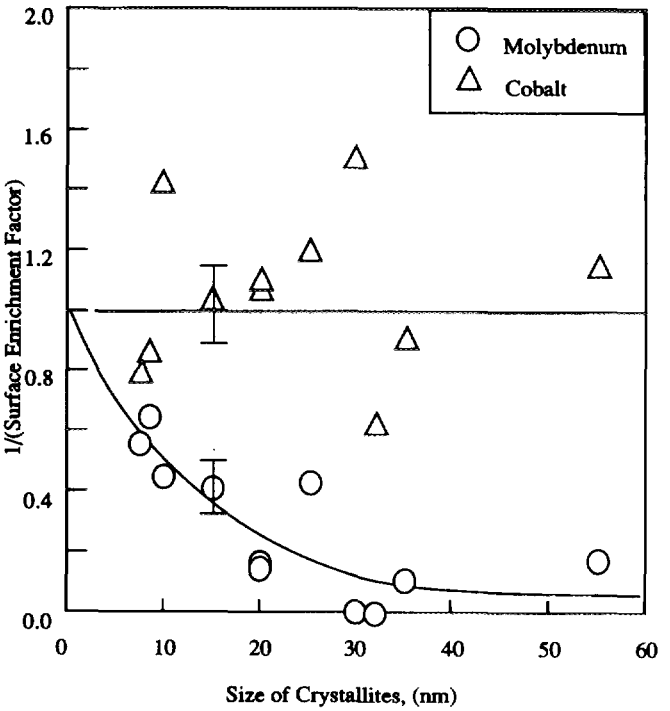


FIG. 7. Effect of crystallite sizes on segregation.

*Characterization by HRTEM*

Figures 8a and 8b show some TEM micrographs of aged HDS16A catalyst. Typically, we could see many crystallites on the catalyst surfaces, which STEM analysis and XRD confirmed to be $Ni_7S_6$ (9). Many different lattice fringe images can be observed on the micrographs. The {111} reflection ($d$ = 0.575 nm) of $Ni_7S_6$ can be observed within many crystallites as in Fig. 8a. Another set of lattice fringes observed in the figures have spacings of about 0.62 nm that one can relate to the 0.615 nm spacings of the {002} basal planes of $MoS_2$. The structure is made of highly disordered S–Mo–S layers of poorly crystallized $MoS_2$. Due to lattice relaxation, some of the fringe spacings are appreciably larger than 0.615 nm.

Consistent with the results from XEDS analyses, molybdenum sulfide was observed on the surfaces of many of the nickel sulfide crystallites. While most of the nickel sulfide crystallites have one or two layers of molybdenum sulfide on the surfaces, crystallites with as many as five or six layers of molybdenum sulfide were also observed, as the crystallite shown in Fig. 8b. The fringe spacing of 0.33 nm corresponds to the {131} reflection ($d$ = 0.328 nm) of $Ni_7S_6$. For slabs of more than two layers, it is easy to assign them to the basal planes of $MoS_2$.

Figure 9 shows micrographs of $MoS_2$ on the same sample. Figure 9a shows an area with many $MoS_2$ fringes but few signs of the significant presence of $Ni_7S_6$ deposits. $MoS_2$ is well dispersed, and the sizes of the crystallites

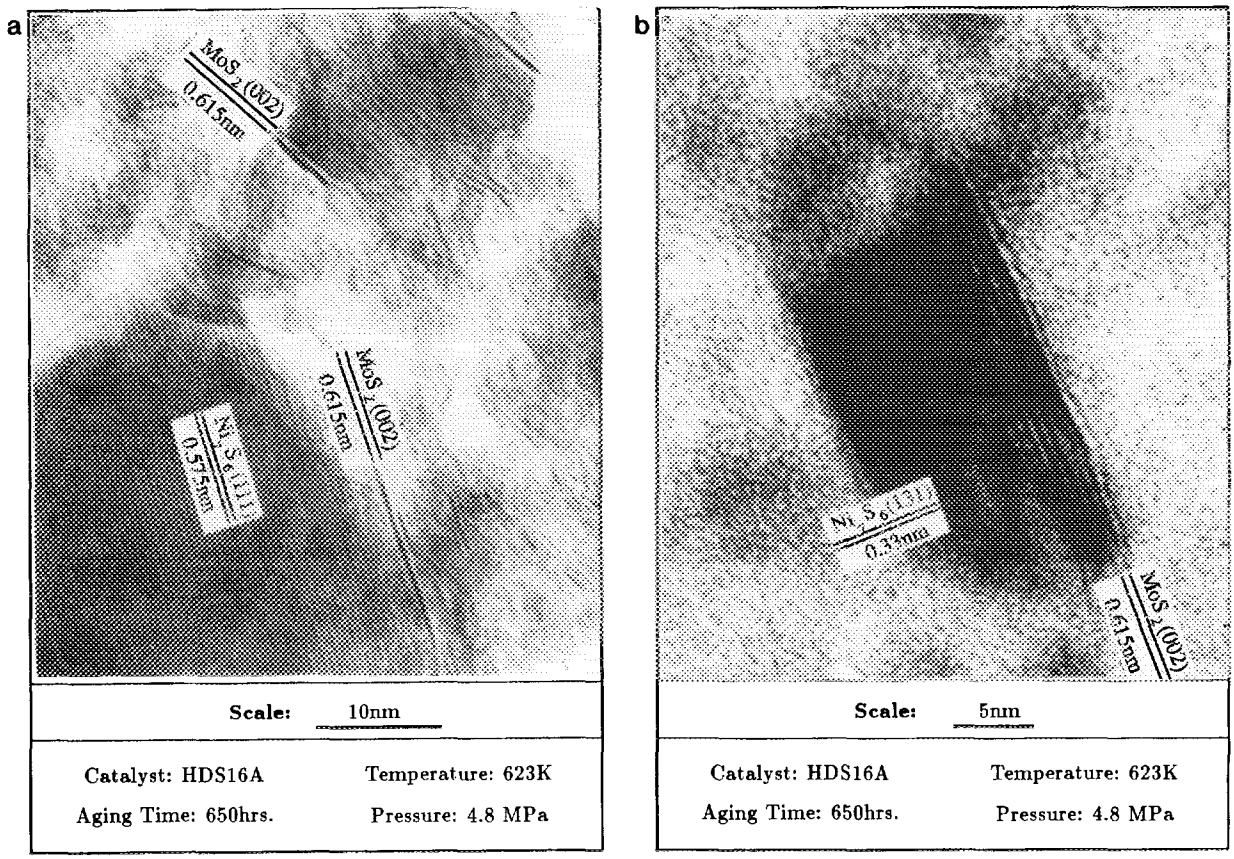


FIG. 8. Lattice fringe image of aged HDS16A catalyst.

are about 10 nm. Figure 9b shows a molybdenum sulfide crystallite. The lattice fringe spacing of 0.28 nm corresponds to the 100 reflection ($d$ = 0.274 nm). The Moirè fringe is probably caused by the overlapping of two crystals. The hexagonal shape of the crystal is very well defined. The size of the crystal is about 30 nm. Although a crystal this size is a rarity, the size of the crystal is very significant.

No lattice fringes are definitely assigned to $Co_9S_8$, partly due to the fact that the main reflections {111} ($d$ = 0.573 nm) and {002} ($d$ = 0.496 nm) of $Co_9S_8$ are difficult to differentiate from reflections of $Ni_7S_6$ ($d_{111}$ = 0.575 nm, $d_{002}$ = 0.470 nm). The difficulty of locating lattice fringes of $Co_9S_8$ could also be explained by the formation of solid solution between $Co_9S_8$ and $Ni_7S_6$. Many fringe images with spacing at 0.15 to 0.2 nm can be observed in the figures, though it is difficult to assign them to a particular compound.

*Discussion*

Surface segregation in metallic alloys and metal oxides has been studied extensively in material science (10). There are several possibilities for the microstructure of such systems. One phase or one component could be enriched on the surface of the crystallites. When an alloy contains two phases in equilibrium, the phase with the lower sublimation energy tends to form the outer surface (11, 12).

$MoS_2$ is one of the transition metal dichalcogenides, which belong to a large class of the so-called two-dimensional solids. They are called two dimensional because they are formed in layered structures. Atoms within a layer are bound by strong covalent or ionic forces, while individual layers are held together by relatively much weaker forces. The latter are frequently referred to as van der Waals type of interaction. Due to the special layered structure of $MoS_2$, it can be very readily cleaved along the basal plane. From a quasichemical point of view, surface energy of solid is determined by the total bonding energy involved when the surface is formed. Therefore, we know that $MoS_2$ would have a much lower surface energy when being cleaved along the basal plane.

The other two sulfides involved in the present system have cubic or orthorhombic structures. There are no special cleavage planes for such structures. Thus, when the three solids are present in a system, molybdenum sulfide

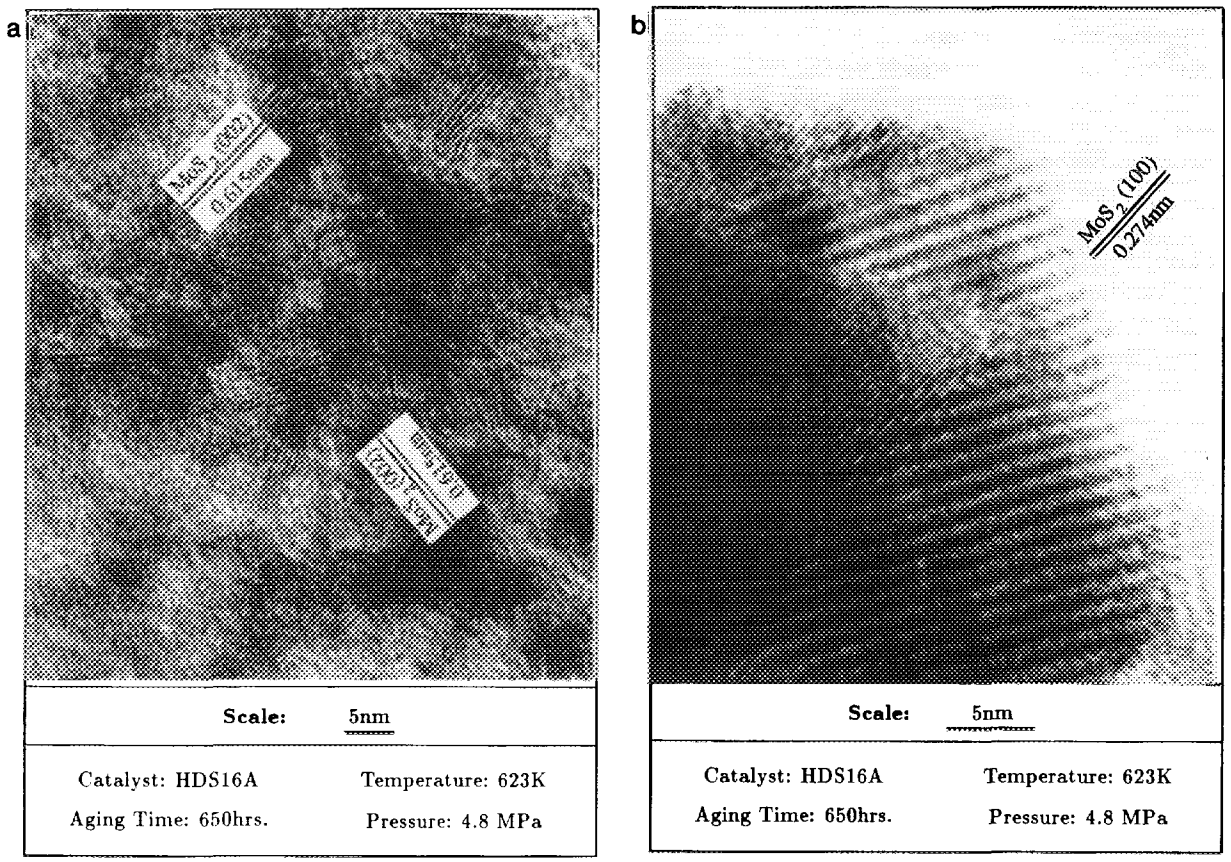


FIG. 9. High-resolution $MoS_2$ image on aged sulfided catalyst.

would be expected to be segregated onto the surface to achieve the minimum of energy of the total system.

Summarizing the electron microscopic observation and the discussion, we can roughly portray the aged catalyst surface with the following physical picture. The metal sulfides on the catalyst surface form three different entities. Most of the nickel sulfide deposits are associated with cobalt sulfides, forming uniform crystallites. For most of the nickel–cobalt sulfide crystallites, a surface layer of molybdenum was observed. This part of molybdenum accounts for about 25% of the total molybdenum on the catalyst surface. The rest of the molybdenum is not directly associated with the nickel deposits; although this part of the molybdenum sulfide is still well dispersed, crystallites with sizes up to 30 nm were occasionally observed.

By using X-ray photoelectron spectroscopy, Fleisch *et al.* found that the ratio of Mo/Al changes with the increase in metal deposits (13). They speculated that molybdenum might have migrated to the top of the contaminated layers and remained exposed to reactants. The present work directly showed that molybdenum sulfide is segregated on the surface of the nickel sulfide deposits due to its lower surface energy.

## DEPOSITION MECHANISM

So far we have shown that nickel deposits are strongly associated with cobalt on the catalyst, while molybdenum sulfide is partially segregated on the surface of the nickel sulfide crystallites. The association of nickel with cobalt could be due to catalytic activity of cobalt sulfide on the catalyst or migration of nickel deposits towards cobalt sites.

It is generally accepted that the active component for hydrodesulfurization and hydrodenitrogenation is molybdenum sulfide with cobalt as a promoter, though there is no general agreement on the structure and functionality of cobalt (14). Few data are available for hydrodemetallation. Hung (15) conducted hydrodemetallation activity studies on a series of $CoO–MoO_3/Al_2O_3$ with different cobalt or molybdenum contents. It was shown that $Mo/Al_2O_3$ catalyst is more active for hydrodemetallation reaction than $Co/Al_2O_3$ catalyst. In fact, the addition of cobalt to a molybdenum catalyst actually reduced the activity of molybdenum catalyst. Therefore, it is unlikely that cobalt acts as the sole active entity for hydrodemetallation on $CoMo/Al_2O_3$ catalysts. A plausible explanation for the association of nickel with cobalt is that the nickel

sulfide preferentially migrates to cobalt sites after being deposited on the catalyst surface.

To confirm the migration of nickel on the catalyst surface, the following experiment was designed. We deposited 10 wt.% of nickel on catalyst HDS16A by impregnating the catalyst with nickel nitrate solution. The catalyst was then calcinated at 773 K for 8 h under a slow flow of air. X-ray elemental mapping and XEDS analysis were then conducted on a scanning transmission electron microscope (STEM).

Elemental mapping of impregnated catalyst samples showed that the crystallites of nickel and the catalytic metals, or Mo and Co, are all very well dispersed on the surface. A typical crystallite measures about 1.5 to 2 nm, though that is the limit of the STEM instrument. XEDS analysis was then conducted on the sample. Since the sizes of the crystallites of the metal sulfides on the catalyst surface are very small, we did not attempt to identify any individual crystallites on the surface. Instead, we positioned the probe on some random positions and conducted EDS analyses. The results shown in Fig. 10 include analyses from four separate catalyst particles. The local nickel loading is independent of local molybdenum/cobalt ratio. In other words, there is no preference of nickel to either cobalt or molybdenum.

The catalyst samples with impregnated nickel were then put into an autoclave reactor under the same conditions as for hydrodemetallation experiments for 200 h, at 648 K and a hydrogen pressure of 4.8 MPa with 0.3 vol.% of hydrogen sulfide. The aim was to observe the development of the deposits on the catalyst surface.

After the 200-h treatment, the sample was taken out for XEDS analysis on a scanning transmission electron microscope. The analysis results shown in Fig. 11 were from 28 sets of analyses on 5 separated catalyst particles. We can clearly see a different trend from the one before

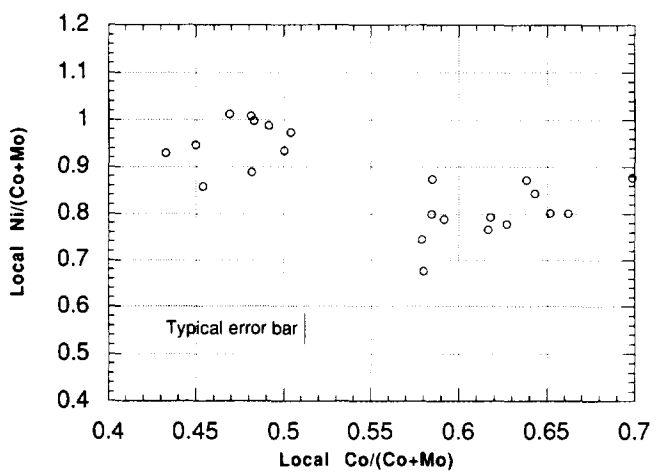


FIG. 10. Microanalysis of HDS16A with impregnated nickel.

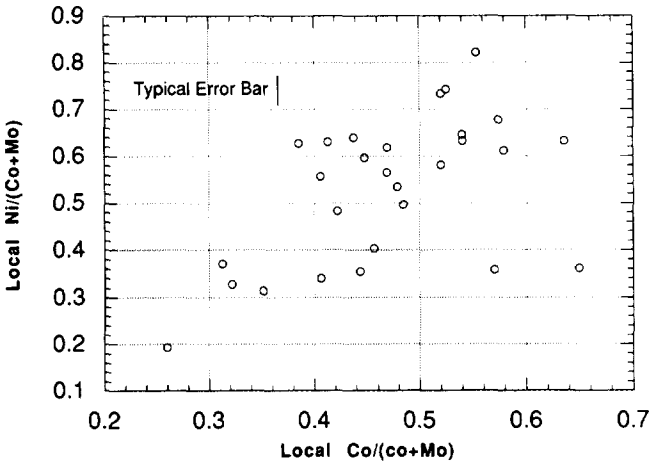


FIG. 11. Microanalysis of HDA16A with impregnated nickel after being treated.

the treatment. Local nickel loading increases with increasing cobalt loading, as was discussed previously (16), which means that nickel has migrated towards cobalt after being treated under hydrodemetallation conditions.

It should be pointed out that the sample after treatment has a slightly lower nickel loading than before treatment. Considering the nickel was impreganted on the catalyst by incipient wetness method and the small numbers of catalyst particles analyzed, the difference might simply be due to the nonuniformity of nickel distribution among different catalyst particles.

The experiment, together with the activity experiment of Hung (15), confirms that subsequent migration, rather than initial deposition on cobalt, causes the association between nickel and cobalt on the aged hydrodemetallation catalyst.

## MOBILITY OF METAL SULFIDES ON CATALYST SURFACE

On aged hydrodemetallation catalyst surfaces, the metal sulfides are distributed in very small microcrystallites. Generally, microcrystallites behave in very different fashions from bulk solids. One particularly important feature is that the melting point of microcrystallite is well below the melting point of a large sample. Tammann temperature, $T_{\mathrm{Tam}}$, which is defined as half of the melting temperature $T_{\mathrm{m}}$ of the bulk solid in degrees K, provides a measure of the extent of mobility of the atoms. It is suggested that the Tammann temperature is associated with a two-dimensional melting of the surface of the solid, i.e., to the transition from a solid to a liquid-like behavior of the surface (16). Baker (17) showed that the mobility of metal and metal oxides has significantly increased mobility above Tammann temperatures.

TABLE 2

**Characteristic Temperatures of Metal Sulfides**

| | $Ni_7S_6$ | $Co_9S_8$ | $MoS_2$ |
|---|---|---|---|
| $T_{Melting}$ (K) | 1063 | 1373 | 2023 |
| $T_{Tammann}$ (K) | 532 | 686 | 1011 |

Order of mobility:
$Ni_7S_6 > Co_9S_8 > MoS_2$

Table 2 shows the melting points and Tammann temperatures of the relevant compounds in the hydrodemetallation system. It should be pointed out that neither $Ni_7S_6$ nor $Co_9S_8$ is stable under the listed melting point temperature, which simply indicates the temperature under which the sulfides becomes liquid. The temperatures are obtained from the respective phase diagrams in Ref. (18). The hydrodemetallation temperature range of 588–623 K is well over the Tammann temperature of nickel sulfide. As a consequences, we expect that nickel sulfide should be mobile on the catalyst sulface.

Tammann temperatures of molybdenum sulfide and cobalt sulfide are both higher than respective hydrodemetallation temperatures. We would not expect an appreciable thermal sintering if the metal sulfides do not interact with each other on the catalyst surface. However, it has been shown that the presence of some components not only strongly affected the shape of metal particles on substrate, but also the surface mobility. Bettler *et al.* (19) and Pichaud and Drechsler (20) showed that silica blocked the migration of tungsten, whereas a monolayer of nickel atoms strongly increased the surface mobility of tungsten. It was suggested that the low melting point of tungsten–nickel alloy caused the increasing mobility of molybdenum.

If we apply the concept of Tammann temperature to a two-phase liquid–solid diagram, we would get a hypothetical phase diagram for the mobility of the components. Figure 12 schematically shows the mobility for two different two-component systems. It resembles two-component liquid–solid phase diagrams except that points A and B represent the Tammann temperatures, rather than melting points, of the two end components. At a temperature between the two Tammann temperatures, the system could be completely mobile in region I, partially mobile in region II, or immobile in region III, depending on the weight percentage of the end component with lower Tammann temperature.

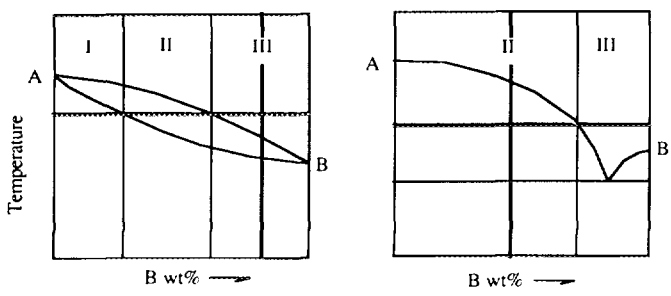


FIG. 12. Mobility regions on hypothetical phase diagrams.

Although we do not have a phase diagram for $Ni_7S_6$ and $Co_9S_8$ at the hydrodemetallation temperature, we do have some relevant information. A Ni–Co–S phase diagram showed that nickel sulfide and cobalt sulfide are completely soluble in each other for a wide range of composition at 1273 K (21). In addition, Co–Ni alloy has been studied by using XPS, SIMS, and other techniques, and the two metals form a continuous series of solid solutions close to ideal solutions (22).

For the sake of discussion, let us assume that $Ni_7S_6$ and $Co_9S_8$ form ideal solution as in the left-hand side of Fig. 12, and $Ni_7S_6$ and $MoS_2$ are not soluble in each other as in the right-hand side of Fig. 12. Hydrodemetallation temperatures of 588–623 K are higher than the Tammann temperature of $Ni_7S_6$, while lower than those of both $Co_9S_8$ and $MoS_2$. Although neither $Co_9S_8$ nor $MoS_2$ would be mobile without the presence of nickel deposits, both of them could become mobile with sufficient amounts of nickel deposits. Molybdenum sulfide is expected to be less mobile than cobalt sulfide for the following two reasons. First, the nickel/molybdenum ratio is much lower than the nickel/cobalt ratio on the catalyst surface. Second, the Tammann temperature of molybdenum sulfide is much higher than that of cobalt sulfide.

In order to substantiate the effect of nickel deposits on the mobility of molybdenum and cobalt sulfide on the catalyst, we will compare the difference between a bare sulfided catalyst, a thermally aged catalyst, and a catalyst subjected to hydrodemetallation here.

### *Sulfided Bare Catalyst*

The structure of sulfided $CoMo/Al_2O_3$ catalyst has been studied extensively by using HRTEM (23–25). Figure 13 shows a high-resolution micrograph of a sulfided HDS16A catalyst sample. We can clearly see that lattice fringe of $MoS_2$ ($d_{002}$ = 0.615 nm) randomly oriented on the catalyst. The sizes of the molybdenum sulfide slabs are usually about a few nanometers in length. The average numbers of the S–Mo–S layers are about four. We tried in vain to locate separate crystals of $Co_9S_8$. The difficulty of observing $Co_9S_8$ may be associated with the low intensity of the main reflections of $Co_9S_8$ crystals. Comparatively, the existence of a strong (002) reflection for $MoS_2$ made in relatively easier to be observed and to be distinguished

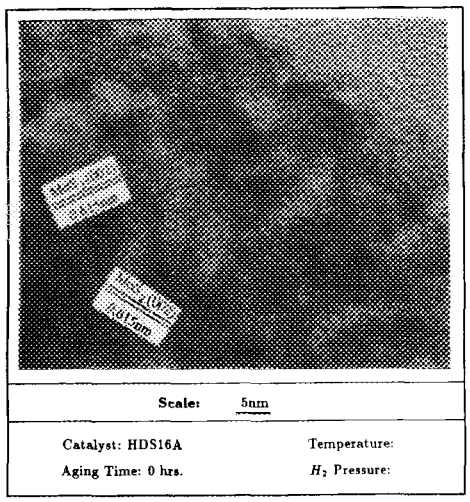


FIG. 13. Lattice fringe image of bare HDS16A catalyst.

from other crystals. Thus, the absence of electron microscopic evidence does not rule out the existence of tiny $Co_9S_8$ crystals.

*Thermally Aged Catalyst*

Figure 14 shows a high-resolution micrograph of a sulfided HDS16A catalyst subjected to thermal aging for about 200 h at 648 K, under the same $H_2S/H_2$ environment as the hydrodemetallation condition, but with no oil or porphyrin. The relatively higher temperature was intended to compensate for the shorter aging time compared to the samples aged with nickel deposits at 623 K for about 600 h. The thermally aged catalyst still very much resembles the unaged catalyst. Many randomly oriented

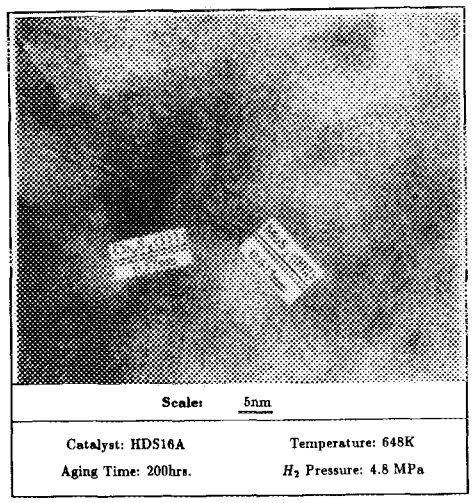


FIG. 14. High-resolution TEM micrograph of thermally aged catalyst.

$MoS_2$ fringes are observed. It appears that the numbers of the S–Mo–S layers and the lengths of the slabs are both slightly increased. No quantitative analysis was attempted. A survey of many areas on HRTEM yields one clear $Co_9S_8$ crystal shown in the lower left corner of the picture. The size of the crystal is about 25 nm. It should be emphasized again that $Co_9S_8$ crystals of this size were not readily observed. Although it is not necessarily conclusive from the observation itself, the mobility of cobalt sulfide, judging from their Tammann temperatures, should be much higher than that of molybdenum sulfide.

*Nickel Aged Catalyst*

The characteristics of the hydrodemetallation reaction aged catalysts have been discussed in the previous sections. Here we want to re-emphasize two additional points. First, the cobalt sulfide phase is completely incorporated into the crystallites of nickel sulfide deposits, as has been shown in the mapping pictures. The sizes of the cobalt sulfide can be, therefore, considered the same as those of nickel sulfide deposits (Fig. 1). Second, there exist two forms of molybdenum sulfide. One form is the molybdenum sulfide associated with nickel deposits as a segregated surface layer. Since it encompasses the nickel crystallites, the lengths of the molybdenum sulfide layers are significantly longer than the slabs on the original catalyst prior to nickel deposition, though there are usually only one to two layers of molybdenum sulfide on the nickel sulfide surface. The other form of the molybdenum sulfide is not associated with nickel and is separately situated on the substrate. These $MoS_2$ crystallites are certainly larger than those on the bare sulfide catalyst or the thermally aged catalyst. If we assume the original slabs of molybdenum sulfide are about 5 nm in length and about 2.5 nm in thickness, it takes over 3000 of them to coalesce to get a crystal over 30 nm in length, as shown in Fig. 9b. The same, of course, is also true for the large crystallites of cobalt sulfide coexisting with nickel deposits, which could be easily found on the mapping pictures.

*Discussion*

In order to form solid solutions between two components, the two components have to be compatible in atomic scale. Field strength can be used to characterize the extent of solid solutions among metal oxides or metal sulfides, and is defined as cation valence divided by the square of cation–anion distance ($Z/d^2$) (26). The extent of solid solution formation decreases with the increase of $\Delta(Z/d^2)$, the difference in field strength of the end-member cations. As expected, the extent of solid solution is at a maximum when $\Delta(Z/d^2) = 0$, and decreases rapidly as $\Delta(Z/d^2)$ increases. When $\Delta(Z/d^2)$ is less than 10%, exten-

TABLE 3

Field Strength of Metal Sulfides

| | Cation ionic radii (Å) | Anion ionic radii (Å) | Cation valence | Field strength | Difference (%) |
|---|---|---|---|---|---|
| $Ni_7S_6$ | 0.69 | 1.70 | +2 | 0.350 | |
| $Co_9S_8$ | 0.72 | 1.70 | +2 | 0.342 | 2.3% |
| $MoS_2$ | 0.79 | 1.70 | +4 | 0.645 | 84.3% |

sive or complete solid solution takes place. When $\Delta(Z/d^2)$ is larger than 0.4, there are virtually no solid solutions.

In the present system, there exist three metal sulfides on the aged catalyst surface: $Ni_7S_6$, $Co_9S_8$, and $MoS_2$. As shown in Table 3, the difference of field strength between $Ni_7S_6$ and $Co_9S_8$ is much less than 10%, and thus extensive formation of solid solution between the two is expected. On the other hand, the difference between $MoS_2$ and the other two sulfides is significantly larger; therefore, little solid solution can be expected.

Another factor determining the extent of solid solution formation between two solids is their structures. Compared with the cubic structure of cobalt sulfide, molybdenum sulfide has a layered hexagonal structure, while nickel sulfide has an orthorhombic structure with structure parameters very close to those of the cobalt sulfide.

## CATALYST DEACTIVATION

In addition to pore plugging to retard diffusion, *covering up of active sites by metal deposits* is the most widely cited cause for the deactivation of hydrodemetallation catalysts. We have shown that nickel deposits do *not* cover up the active component molybdenum disulfide. The covering up of cobalt sulfide sites is irrelevant to the catalyst deactivation. Whatever role cobalt was playing for the original catalyst, nickel is readily available as the substitute. As a matter of fact, the data of Smith and Wei (2) showed that the catalyst kept virtually the same activity for nickel loading up to about 60%, though nickel deposits only possess about one-tenth to about one-third of the activity of cobalt-promoted molybdenum catalyst (27).

We suggest that enhanced sintering due to the deposition of nickel on the catalyst is an important factor for catalyst deactivation. Naturally, the coalescence of small crystallites into larger ones causes significant reduction of molybdenum sulfide surfaces accessible to the reactant. Another factor that should be considered is the decreasing of the number of edge sites with the sintering of molybdenum sulfide. It is generally accepted that the edge sites, instead of basal sites, of molybdenum sulfide are the catalytic sites. In addition to the reduction of edge sites by the coalescence of molybdenum sulfide, the part of molybdenum sulfide segregated on the nickel sulfide would also have fewer edge sites available than an unaged catalyst. This is due to the fact that the surface layer usually has a much larger patch, though it is a very thin layer. Therefore, the ratio of edge/basal sites is significantly reduced by the enhanced sintering of the catalytic components. This mechanism may be controlling the second stage of the catalyst deactivation process.

One of the conclusions from the *random sphere model* proposed by Smith and Wei (5) was that segregated large crystallites of nickel deposition lead to less deactivation, in comparison with uniform layers of nickel deposition. Based on the present study, one possibility of controlling the deposition pattern is to control the morphology of cobalt sulfide on the catalyst. Because of the strong association between nickel and cobalt sulfide on the catalyst, it might be possible to achieve large segregated crystallites of nickel deposits simply by adding less cobalt to the original catalyst. For hydrodesulfurization reaction, the purported synergic effect between cobalt and molybdenum requires the existence of cobalt. For hydrodemetallation reaction, the addition of cobalt might not be highly necessary. First, less cobalt might be able to lead to less nucleation sites for nickel deposits. Second, whatever role requires cobalt can always be fulfilled using nickel as a substitute.

Available literature information supports the above suggestion. Hung (15) showed that the addition of cobalt to a molybdenum catalyst actually decreases its hydrodemetallation activity. Another set of data is from Hisamitsu *et al.* (28). It was shown that, although cobalt or nickel had a significant promoter effect for hydrodesulfurization reactions, the promoter effect was much less significant for hydrodemetallation reactions. On the other hand, the addition of cobalt caused a significant acceleration of the deactivation rate. The authors concluded that the addition of cobalt or nickel was considered to be disadvantageous as far as hydrodemetallation was concerned. The promoter effect of cobalt was also reported by Morales *et al.* (29) to be minimal for hydrodemetallation.

## CONCLUSIONS

- Nickel sulfide deposition and cobalt sulfide on the catalyst are strongly associated with each other. Within the crystallite, cobalt sulfide and nickel sulfide are uniformly distributed.
- Contrary to the uniform distribution of cobalt, molybdenum sulfide is strongly enriched on the surface of the crystallites formed by nickel deposits with cobalt sulfide. The molybdenum associated with nickel deposits as a

segregated surface layer accounts for about 25% of the total molybdenum on the catalyst surface. The rest of the molybdenum sulfide is not directly associated with nickel deposits.

- Extensive cover up of molybdenum sulfide by nickel deposits is not observed, and is not a main mechanism for hydrodemetallation catalyst deactivation.
- The association of nickel sulfide deposits on the aged hydrodemetallation catalyst is due to the subsequent migration of nickel sulfide deposits rather than to the initial deposition on the cobalt sites.
- The mobilities of cobalt and molybdenum are significantly enhanced by the presence of nickel deposits. The increasing mobility was caused by the lowering of the Tammann temperatures of $Co_9S_8$ and $MoS_2$.
- The nickel-enhanced coalescence of molybdenum sulfide leads to a significant reduction of accessible molybdenum sites, and is a main reason for the deactivation of hydrodemetallation catalysts. It is suggested that a catalyst with less cobalt would be expected to be as active for hydrodemetallation reaction as the present catalyst, but slower in deactivation.

## ACKNOWLEDGMENTS

The financial support of Mobile Oil Research and Development Corporation and Chevron Research Company is gratefully acknowledged. The authors also thank Dr. J. D. Carruthers and Dr. R. H. Whitman of American Cyanamid at Stamford, Connecticut for providing catalyst samples. The assistance and various help of Dr. Anthony J. Garratt-Reed and Mr. Michael Frongillo on electron microscopy are greatly appreciated.

## REFERENCES

1. Nourbakhsh, N., Smith, B. J., Webster, I. A., Wei, J., and Tsotris, T. T., *J. Catal.* **127,** 178 (1991).
2. Smith, B. J., and Wei, J., *J. Catal.* **132,** 21 (1991).
3. Toulhoat, H., Plumail, J. C., Martino, G., and Jacquin, Y., *in* "ACS Div. Petrol. Chem., Symposium on Advances in Resid Upgrading, Denver, 1987."
4. Smith, B. J., and Wei, J., *J. Catal.* **132,** 1 (1991).
5. Smith, B. J., and Wei, J., *J. Catal.* **132,** 41 (1991).
6. Wei, J., and Zhao, X., *Chem. Eng. Sci.* **47,** 2721 (1992).
7. Speight, M., "The Desulfurization of Heavy Oils and Residue." Dekker, New York, 1981.
8. Helms, C. R., *in* "Interfacial Segregation: Papers Presented at a Seminar of the Materials Science Division of the American Society for Metals, October 22 & 23, 1977" (W. C. Johnson and J. M. Blakely, Eds.), p. 175. Books on Demand, Ann Arbor, MI, 1977.
9. Zhao, X., D.Sc. thesis, Massachusetts Institute of Technology, 1992.
10. Nowotny, W., and Dufour, L. C., "Surface and Near Surface Chemistry of Oxide Materials." Elsevier, Amsterdam, 1988.
11. Haber, J., *in* "Catalysis: Science and Technology" (J. R. Anderson and M. Boudart, Eds.), Vol. 2, p. 14. Springer-Verlag, New York/Berlin, 1981.
12. Biswas, J., Bickel, G. M., Gray, P. G., Do, D. D., and Barbier, J., *Catal. Rev.—Sci. Eng.* **30,** 161 (1988).
13. Fleisch, T. H., Meyers, B. L., Hall, J. B., and Ott, G. L., *J. Catal.* **86,** 147 (1984).
14. Prins, R., de Beer, V. H. J., and Somorjai, G. A., *Catal. Rev.—Sci. Eng.* **31,** 1 (1989).
15. Hung, C. W., Ph.D. thesis, Massachusetts Institute of Technology, 1979.
16. Satterfield, C. N., "Heterogeneous Catalysis in Practice." McGraw-Hill, New York, 1991.
17. Baker, R. T. K., *J. Catal.* **78,** 473 (1982).
18. Massalski, T. B., "Binary Alloy Phase Diagrams," 2nd ed. ASM International, Materials Park, OH, 1990.
19. Bettler, P. C., Bennum, B. H., and Case, C. M., *Surf. Sci.* **44,** 360 (1974).
20. Pichaud, M., and Drechsler, M., *Surf. Sci.* **36,** 813 (1973).
21. Jacob, K. T., *Metall. Trans., B* **11B,** 640 (1980).
22. Minachev, Kh. M., and Shpiro, E. S., "Catalyst Surface: Physical Methods of Studying." CRC Press, Boca Raton, 1990.
23. Delannay, F., *Appl. Catal.* **16,** 135 (1985).
24. Delannay, F., Gajardo, P., Grange, P., and Delmon, B., *J. Chem. Soc., Faraday Trans.* **76**(5), 988 (1980).
25. Pratt, K. C., Sanders, J. V., and Christov, V., *J. Catal.* **124,** 416 (1990).
26. Berkes, J. S., and Roy, R., *Z. Kristallogr.* **131,** 60 (1970).
27. Chianelli, R. R., *Catal. Rev.—Sci. Eng.* **26,** 361 1984.
28. Hisamitsu, T., Komori, K., and Ozaki, H., *in* "Catalyst Deactivation: Proceedings" (B. Delmon and G. F. Froment, Eds.), p. 259. Elsevier, Amsterdam/New York, 1980.
29. Morales, A., Martinez, N. P., Laine, J., and Grimblot, J., *Appl. Catal.* **6,** 329 (1983).